Heliyon 10 (2024) e39858

Contents lists available at ScienceDirect

Heliyon

journal homepage: www.cell.com/heliyon

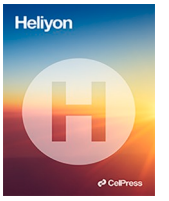

Research article

IMM2520, a novel anti-CD47/PD-L1 bispecific antibody for cancer immune therapy

Chunmei Yang [a,1], Song Li [a,1], Dianze Chen [a,1], Dandan Liu [a], Yanan Yang [a], Huiqin Guo [a], Nana Sun [a], Xing Bai [a], Guanghui Li [a], Ruliang Zhang [b], Tianxiang Wang [b], Li Zhang [b], Liang Peng [b], Sijin Liu [b], Wei Zhang [b], Gui Zhao [b], Xiaoping Tu [b], Wenzhi Tian [a,b,*]

[a] Department of R&D, ImmuneOnco Biopharmaceuticals (Shanghai) Inc., Shanghai, 201203, China
[b] Department of CMC, ImmuneOnco Biopharmaceuticals (Shanghai) Inc., Shanghai, 201203, China

ARTICLE INFO

Keywords:
PD-L1
CD47
Bispecific antibody
IMM2520
Immune therapy
Antitumor activity

ABSTRACT

PD-1/PD-L1 is an important signaling pathway in the adaptive immune system. The CD47/SIRPα signaling pathway is a crucial "do not eat me" signal for innate immunity. This study evaluated the anti-tumor mechanism of IMM2520 *in vitro* and *in vivo*. IMM2520 was generated using the "mab-trap" platform. IMM2520 showed high affinity to PD-L1 and relatively lower affinity to CD47, displaying preferential binding to PD-L1 on tumor cells. IMM2520 had the potent ability to inhibit the PD-1/PD-L1 and CD47/SIRPα signaling pathways and killed tumor cells through ADCC and ADCP. Importantly, IMM2520 did not bind to human red blood cells or induce erythrocyte agglutination. IMM2520 demonstrated a tendency to bind to $CD47^{+}$/$PD\text{-}L1^{+}$ tumor cells, reducing its binding to CD47 single-positive cells. In mouse transplantation models, compared with the first-generation CD47/PD-L1 BsAb (IMM2505), IMM2520 exhibited stronger and dose-dependent antitumor activity. These findings imply that IMM2520 may offer a novel therapeutic alternative for cancer patients.

1. Introduction

The prevalence of cancer poses a major challenge for public health. The latest Global Cancer Statistics report for 2022, there is an estimated incidence of nearly 20 million new cases worldwide (19.96 million cancer patients if non-melanoma skin cancer is included and 18.73 million cancer patients if non-melanoma skin cancer is excluded), with approximately 9.7 million deaths attributed to this disease [1]. The immune system relies on tumor immune surveillance, an important mechanism that actively monitors, identifies, and eliminates pre-cancerous or cancerous cells within the body [2]. However, the tumor cells use mechanisms of tumor immunoediting and immune tolerance to evade immune surveillance; thereby allowing the tumors to continue developing despite normal immune system function [3,4]. Therefore, the utilization of immune checkpoint inhibitors (ICI) in the management of malignant neoplasms has emerged as a pivotal therapeutic option.

* Corresponding author. ImmuneOnco Biopharmaceuticals (Shanghai) Inc., Building 15, Lane 1000, Zhangheng Road, Zhangjiang Science City, Pudong New Area, Shanghai, China.
E-mail address: wenzhi.tian@immuneonco.com (W. Tian).
[1] These authors contributed equally to this work as the Co-first author.

https://doi.org/10.1016/j.heliyon.2024.e39858
Received 10 April 2024; Received in revised form 17 October 2024; Accepted 24 October 2024
Available online 26 October 2024

Among the representative drugs for cancer immunotherapy, programmed death 1/programmed cell death-Ligand 1 (PD-1/PD-L1) antibody drugs have demonstrated great success in treating various malignant tumors. PD-1 is expressed on activated T cells and has been extensively investigated for its potent immunosuppressive effects [5]. PD-L1 is expressed on a variety of tumor cells and participates in the PD-L1/PD-1 signaling pathway, ultimately inhibiting T cell activity and effectively evading immune system surveillance [6,7]. The utilization of therapeutic antibodies targeting PD-1 or PD-L1 can effectively reinstate the tumor immune response, thereby accomplishing tumor control and eradication [8,9]. The efficacy of PD-1 or PD-L1 targeting antibodies is restricted in certain cancer patients, leading to an unfavorable prognosis [10]. The exploration of combinations involving different immune checkpoint blocking antibodies, such as Cytotoxic T-Lymphocyte Antigen 4 (CTLA-4), vascular endothelial growth factor (VEGF), have been explored, and the implementation of these measures leads to a substantial enhancement in patient response rates and an extension of survival duration [11,12]. However, the adoption of combination therapy with ICIs presents new options for patients with tumor while potentially inducing varying degrees of side effects in clinical practice, termed immune-related side effects [13,14]. Therefore, in addition to exploring suitable combinations of other immune checkpoint inhibitors (ICIs), the crucial aspect lies in prioritizing the advancement of these groundbreaking therapies, specifically T cell-targeted bispecific antibodies. Bispecific antibodies, including PRS-343 (HER2 × 4-1BB), MCLA-145 (PD-L1 × 4-1BB), and FS118 (PD-L1 × LAG-3), possess the ability not only to activate immune cells' anti-tumor activity but also directly induce tumor cell apoptosis [15]. The capacity of bispecific antibodies to activate tumor-infiltrating T cells that are already present in the tumor microenvironment (TME) and elicit a gradual and enduring immune response enhances the specificity and safety profile of these therapeutic agents [16].

The cell surface protein CD47, which serves as a crucial target in tumor therapy, is abundantly expressed on various types of tumor cells. It functions by engaging its receptor signal regulatory protein alpha (SIRP alpha) to transmit an inhibitory "Don't eat me" signal to macrophages, thereby effectively suppressing phagocytosis [17,18]. However, the presence of CD47 is not limited to malignant cells, it is also found in numerous non-malignant cells, particularly erythrocytes and thrombocytes [19,20]. The current focus of preclinical and clinical studies lies in the development of multiple therapeutic antibodies that target CD47 or SIRPα. But most CD47-targeting drugs have demonstrated limited single-agent efficacy against tumors. Monotherapy of Magrolimab (NCT02216409), the first-in-class anti-CD47 antibody with IgG4 component, demonstrated partial tumor remission in only two out of 62 patients with advanced solid malignancies or lymphomas [21]. The investigation of CC-90002 (NCT02641002), an additional CD47-targeting antibody, in a cohort of 28 patients with relapsed/refractory acute myeloid leukemia (AML) or high-risk myelodysplastic syndrome (MDS), and was terminated due to insufficient monotherapy activity [22]. Consequently, CD47-based combination strategies may potentially generate more favorable outcomes. The current cancer immunotherapies available primarily stimulate innate or adaptive immunity by means of immune checkpoint antibodies. The findings of this study suggest that selectively eliminating Treg cells from the tumor microenvironment can be effectively achieved by targeting CTLA-4 and CD47 on Treg cells using SIRP-α × anti-CTLA-4 heterodimers [23]. The aforementioned method not only enhances "eat me" signal, but also suppresses "don't eat me" signal, resulting in a more pronounced effect. The findings suggest that exploiting intrinsic checkpoints of adaptive immune regulatory cells could serve as a strategic approach in the development of efficacious and safe immunotherapies for solid tumors [23]. The CD47/SIRPα and PD-L1/PD-1signaling pathways, representative of innate and adaptive immunity suppression, are important players in cancer immune evasion [24]. Therefore, targeting both pathways simultaneously presents a promising solution for cancer treatment. The therapeutic efficacy has been validated in animal models, and simultaneous targeting of the CD47/SIRP α and PD-1/PD-L1 pathways can yield favorable outcomes [25]. The bispecific antibody IBI322 (NCT04795128), targeting both PD-L1 and CD47, was assessed in a clinical trial, demonstrating favorable tolerability and safety profiles alongside significant antitumor efficacy in 24 patients with classical Hodgkin lymphoma who had previously failed PD-1 or PD-L1 antibody therapy [26].

The bispecific antibody IMM2520 was developed in this study, which consists of the first domain of SIRPα linked to the N-terminal region of the heavy chain of PD-L1 monoclonal antibody. The specific target of IMM2520 is CD47 on tumor cells, thereby alleviating the inhibitory effect of tumor cells on macrophages. IMM2520 effectively disrupts the PD1/PD-L1 signaling pathway by specifically targeting PD-L1 on tumor cells, thereby attenuating T cell immunosuppression. The binding of IMM2520 to the Fc-γ receptor produces antibody-dependent cell-mediated cytotoxicity (ADCC) and antibody-dependent cell-mediated phagocytosis (ADCP), thereby enhancing its immunological effects. The effective therapeutic effect of IMM2520 was demonstrated in various murine models. Furthermore, *in vitro* assessments revealed no affinity of IMM2520 towards human or rhesus erythrocytes.

2. Materials and methods

2.1. Cell lines

The Jurkat, Raji, RKO, ES-2, HT-1080, HCC827, and THP-1 cell lines were purchased from the cell bank of the Chinese Academy of Sciences. CHO-PD-L1, CHO-GSKO-4B3, MC38-hPD-L1KI, Raji-PD-L1, and FcgRIIIA (158V) target activated NK (FcR-TANK) cells, were constructed in our laboratory. CHO-PD-L1 cells were cultured in EX-CELL® 302 serum-free medium for CHO cells (Cat#24326C-50L; Sigma) supplemented with 1 % penicillin-streptomycin (Cat#15140122; Gibco). Jurkat, Raji, Raji-PD-L1, RKO, ES-2, HT-1080, HCC827, and THP-1 cell lines were cultured at 37 °C and 5 % CO_2 in RPMI-1640 medium (Cat#11875093; Gibco) supplemented with 10 % fetal bovine serum (Cat#KC001–01; KEL) and 1 % penicillin-streptomycin. FcR-TANK cells were cultured using TANK serum-free medium (Cat#CT001–1; ImmuneOnco Biopharmaceuticals). MC38-mCD47KO-hPD-L1KI cells were cultured in Dulbecco's modified Eagle's medium (Cat#12100046; Gibco) containing 10 % fetal bovine serum and 1 % streptavidin.

2.2. Preparation and expression of bispecific antibody

The immunogen used for the immunization of C57BL/6 mice was MC38-hPD-L1KI cells, followed by the preparation of hybridoma cells. The presence of hPD-L1 antibody in the supernatant was detected using enzyme-linked immunosorbent assay (ELISA) and flow cytometry (fluorescence-activated cell sorting [FACS]). Subsequently, a subset of positive samples underwent variable region (VL and VH) gene sequencing using the SMARTer® RACE 5′/3′Kit (Cat#634858; Takara). The PD-L1 antibody was expressed in CHO-S cells, followed by purification using protein A resin(Cat#AA0273; Bestchrom). The purified antibodies underwent various functional analyses, and those demonstrating superior performance were humanized through the implementation of a CDR grafting strategy [27]. The CD47/PD-L1 bispecific antibody IMM2520 was produced by genetically engineering a SIRPα-extracellular first domain to be connected at the N-terminal of the heavy chain of the PD-L1 antibody through a (G4S)3 linker [28]. This construct was then expressed in CHO-K1 cells and purified using protein A resin.

2.3. Antibody quality analysis

The N-glycan of the IMM2520 protein was released, labeled, separated, and detected in the sample using high-performance liquid chromatography (HPLC)-hydrophilic interaction liquid chromatography (HILIC). The N-glycans were analyzed qualitatively and quantitatively based on chromatographic information and glucoside standard data. The isoelectric point and charge heterogeneity of IMM2520 were characterized using full-column imaging capillary isoelectric focusing electrophoresis (iCIEF). The IMM2520 protein was analyzed for polymer content using Molecular Exclusion Chromatography (Size Exclusion Chromatography [SEC]-HPLC), which facilitated the separation of proteins based on their molecular size. Nonreductive capillary gel electrophoresis–sodium dodecyl sulfate (nrCE-SDS) and reductive capillary gel electrophoresis–sodium dodecyl sulfate (rCE-SDS) were used to detect degraded fragment in the IMM2520 protein. Additionally, IMM2520 stability was analyzed using a differential scanning calorimetry (DSC) instrument to determine its Tm value.

2.4. Biolayer interferometry technology analysis of affinity and dual-target binding

2.4.1. Affinity determination assay

The Gator™ Label-Free Bioanalysis instrument (Gator Bio) was employed for the biolayer interferometry (BLI) assay. The measurements were conducted using a set of six probes, including both sample and reference probes. To set up the assay, the anti-His probes (Cat#20–5066; Gator Bio) and the anti-mouse IgG Fc probes (Cat#20–5046; Gator Bio) were pre-incubated for 300 s in Q buffer (10 mM phosphate-buffered saline [PBS] + 0.02 % Tween + 0.2 % bovine serum albumin [BSA]; pH = 7.4). The measurements commenced by conducting a 30-s baseline in the Q buffer using sample probes. The Probe loading was conducted for 120 s utilizing a concentration of 10 μg/mL His-tag PD-L1 antigen (Cat#10084-H08H; Sino Biological) or mFc-tag CD47 antigen (in-house).The subsequent step involved washing the probe in Q buffer for 30 s, followed by incubating the probe in different concentration IMM2520 wells for 120 s (association step), and then another 120 s of probe incubation in Q buffer (dissociation step). The measurement method for the reference probe and the sample probe is identical, with the exception that antibody utilization is not involved. The curve fitting was performed using Gator software after background subtraction.

2.4.2. Dual-target-binding determination assay

The BLI tandem approach was utilized to assess the dual target binding capability of IMM2520. The measurement commenced by establishing a 30 s baseline in Q buffer, utilizing an anti-human IgG probe (Cat#20–5036; Gator Bio). The subsequent steps included loading the probe with 10 μg/mL CD47/PD-L1 antibody for 120 s, rinsing the probe with Q buffer for 30 s, incubating the probe in a well containing 10 μg/mL first antigen for 60 s, and incubating the probe in a well containing 10 μg/mL second antigen along with 10 μg/mL first antigen for 30 s.

2.4.3. Enzyme linked immunosorbent assay

The quantification of the binding between IMM2520 and hPD-L1 as well as hCD47 was performed using an ELISA assay. The hCD47 or hPD-L1 antigen (50 ng/well) was immobilized on a 96-well plate by overnight incubation at 4 °C, followed by sealing at room temperature for 2 h with PBS containing 3 % (w/v) skim milk (Cat# 941500704013; Anchor). The samples underwent dilution to achieve a concentration of 10 μg/mL in the presence of PBS supplemented with 3 % skim milk. Subsequently, the diluted samples underwent triple gradient dilution and were added to a sealed 96-well plate for incubation at 37 °C for 1 h. The plate was subsequently washed with PBS solution supplemented with Tween 20 (diluted at a ratio of 1000-fold; Cat#DH358–4, DING GUO). The samples were then incubated with a 10,000-fold diluted peroxidase-conjugated AffiniPure F $(ab')_2$ fragment goat antihuman IgG, Fcγ fragment-specific antibody (Cat#109–036–098; Jackson Immuno) secondary antibody at 37 °C for 1 h. After the washing step, the TMB substrate (Cat#51200050; KPL) was used to induce color development in a light-restricted environment for a duration of 15 min. The reaction was subsequently terminated by the addition of a 1 mol/L H2SO4 solution. The OD450 value was measured using enzyme-labeled instrument (Sunrise4; Tecan).

2.5. Binding toCD47+/PD-L1+ tumor cells, erythrocytes, PBMCs, and thrombocytes

The binding of antibodies to $CD47^+$/$PD\text{-}L1^+$tumor cells (including Jurkat, CHO-PD-L1, RKO, ES-2, HT-1080, and HCC827), RBCs,

peripheral blood mononuclear cells (PBMCs), and platelets was assessed by flow cytometry. hIgG1-Fc (in-house) was used as an isotype reference. The antibodies were diluted by gradient in PBS supplemented with 0.5 % BSA (Cat#A500023–0100; Sangon Biotech). The antibodies were incubated at 4 °C with cells at multiple serial dilution concentrations for 45 min. Subsequently, free antibodies were washed by PBS supplemented with 0.5 % BSA. The antibodies were subsequently incubated with FITC-linked anti-human IgG Fc secondary antibodies (500-fold dilution; Cat#F9512, Sigma) at 4 °C in the dark for 45 min. After washing, the FITC fluorescence signals of the cells were evaluated using flow cytometry analysis (Luminex, Guava® easyCyte™ 8HT Base System). The acquired data were analyzed using guavaSoft_33_x64 software.

2.6. Blocking PD-1/PD-L1 and CD47/SIRPα interaction assay

The Jurkat, CHO-PD-L1, or RKO cells were incubated with different concentrations of CD47/PD-L1 BsAbs for 45 min. Subsequently, SIRPα-mFc (in-house) or PD1-mFc (in-house) at a concentration of 1 μg/mL was added and incubated for another 45 min. The cells were subsequently rinsed with PBS supplemented with 0.5 % BSA-PBS, followed by the addition of the PE-conjugated anti-mouse IgG secondary antibody (diluted 500-fold; Cat#405307; Biolegend). The PE fluorescence signal of the cell was assessed using flow cytometry analysis.

2.7. In vitro Fc-mediated effector function (ADCC/ADCP) assay

2.7.1. ADCC assay

The target cells were stained with carboxyfluorescein succinimidyl ester (CFSE; 200 nM; Cat#21888; Sigma) and subsequently incubated with samples of varying concentrations for a duration of 30 min. The FcgRIIIA (158V) target-activated NK (FcR-TANK™) effector cells (in-house) were subsequently introduced into the pre-incubated cell pores at a 2:1 E/T ratio and incubated at 37 °C with 5 % CO_2 for 4 h. Subsequently, the cells were subjected to staining with a solution of Propidium Iodide (PI), followed by collection using flow cytometry and subsequent assessment of the ratio of PI-positive target cells. The ADCC intensity was calculated using the formula: Lysis% = [(E + T + Ab)% PI-positive cells − (E + T)% PI-positive cells]/(100 − T% PI-positive cells) × 100 %. E and T are effector cell and target cell, respectively.

2.7.2. ADCP assay

THP-1 cells were harvested and rinsed with RPMI-1640 media supplemented with 1 % penicillin-streptomycin. The THP-1 cells (100 μL; 4×10^5 cells/mL) were cultured with PMA (200 ng/mL; Cat#P-050; Sigma) at 37 °C with 5 % CO2 for a duration of 24 h. The target cells were incubated with 200 nM CFSE at 37 °C for a duration of 30 min, followed by quantification and collection of the target cells. After rinsing twice with complete culture media, the labeled target cells were plated at a density of 1×10^5 cells/well (50 μL, 2×10^6/mL). The cells were incubated with a continuously diluted antibody (effector cells: target cells = 2:5) at a volume of 50μL/well for 2 h in an incubator maintained at 37 °C and 5 % CO_2.The plates were washed with PBS to eliminate any remaining free target cells. Subsequently, the samples were resuspended in PBS, mean fluorescence intensity (MFI) of macrophages were quantified using flow cytometry, and the phagocytic index was defined as the fluorescence intensity of macrophages that engulfed the target cells.

2.8. Cytokine release

IMM2520 was diluted to the initial concentration of 1000 nM using PBS, and subsequently subjected to a triple gradient dilution. The sample was subsequently transferred to a 96-well plate and subjected to incubation at room temperature for a duration of 2 h. Afterward, the plate was washed twice with PBS. PBMCs were isolated from whole blood, their density adjusted to 1×10^6 cells/mL, and then added to the pre-coated 96-well plate with antibodies. The plate was incubated at a temperature of 37 °C for a duration of 24 h. The cell culture supernatant was collected and analyzed using the cytometric bead array (CBA) method to detect ten cytokines, including interleukin-1β (IL-1β), IL-2, IL-4, IL-5, IL-6, IL-8, IL-10, interferon γ (IFN-γ), tumor necrosis factor α (TNF-α), and granulocyte-macrophage colony-stimulating factor (GM-CSF). Human CD3 (humanized OKT3) antibody (Cat#10977-H001; Sino-Biological) and human CD28 antibody (Cat#11524-H001; SinoBiological) were employed as positive control, while hIgG1-Fc was utilized as a negative control.

2.9. In vivo xenograft mouse model

The *in vivo* efficacy of IMM2520 was evaluated in CT26-hPD-L1/hCD47 syngeneic models. Briefly, a suspension of 2×10^6 cells (100 μL) in a PBS/Matrigel mixture with a volume ratio of 1:1 was prepared and subsequently inoculated into the right dorsal region near the axilla of BALB/c-hPD1/hSIRPα mice. After the average tumor volume reached 80 mm^3–100 mm^3, the mice were randomly grouped based on their tumor size and body weight. All experiments were conducted via intraperitoneal injection. The dose-dependent efficacy experiment of IMM2520 was conducted at doses of 0.3, 1, 3 mg/kg, the control group was the solvent dilution of IMM2520 stock solution, and was administered twice weekly for a total of 6 treatments, with 8 mice in each group. Comparative experiment on the efficacy of IMM2520 and IMM2505 (based on the atezolizumab backbone) was conducted at doses of 6 mg/kg, the control group was PBS solution, and was administered twice weekly for a total of 8 treatments, with 6 mice in each group. The body weight and tumor volume of the mice were measured twice per week, and euthanasia was performed when the tumor size reached 3000 mm^3.

2.10. Statistical analysis

The statistical measurements were conducted using GraphPad Prism 8.0 (GraphPad Software Inc.). Differences among three or more groups were analyzed using one-way analysis of variance with Holm-Sidak correction, while differences between individual groups were evaluated using Student's t-tests. A significance level of $p \leq 0.05$ indicated statistically significant differences between the groups.

3. Results

3.1. Design and quality analysis of IMM2520

Recently, we have reported the crystal structure of human CD47 in a complex with engineered SIRPα-extracellular first domain (SIRPαD1) carrying mutation of Asn-80 to Ala [28]. The surface of CD47 is buried by IMM01 (SIRPαD1 Fc fusion protein), so that IMM01 can significantly block theCD47/SIRPα signal. IMM01 effectively suppressed the macrophage "don't eat me" signal while activating the phagocytosis "eat me" signal, thereby exhibiting potent antineoplastic activity and demonstrating a dual mechanism against tumor growth [29]. The bispecific antibody IMM2520 was engineered to connect the SIRPαD1 at the N-terminus of the heavy chain of the PD-L1 antibody (IMM2515H) through a (G4S)3 linker (Fig. 1). The previous literature reports suggest that the incorporation of E333A, S298A, and K334A substitutions in the Fc region of IMM2520 can enhance Fc-mediated effector functions by improving its binding to FcgRIIIA [30]. IMM2520 was produced using a stable expression cell line derived from CHO-K1 cells and subsequently purified utilizing Protein A resin. To ensure its druggability, the protein quality of IMM2520 was thoroughly assessed. The molecular size heterogeneity of IMM2520 was evaluated through SEC-HPLC, nrCE-SDS, and rCE-SDS. SEC-HPLC analysis indicated that the proportion of main peak was 96.71 %. There was no obvious polymer, and the main peak had high purity (Fig. 1B). The nrCE-SDS analysis further confirmed that the IMM2520 main peak constituted 98.6 % of the total, displaying no observable signs of degradation. Subsequent rCE-SDS analysis indicated that the combined proportion of heavy and light chains was 99.2 %, revealing no noticeable breakage in either chain (Fig. 1C). The isoelectric point of IMM2520 was determined using full-column iCIEF, yielding a measured pI value of 8.45, closely aligning with the theoretical value of pI = 8.39 (Fig. 1D). Subsequently, HPLC-HILIC was employed to separate N-sugars to detect any modifications. The results unveiled that IMM2520 displayed a typical IgG sugar type with no complex sialic acid modification and a slightly higher proportion of high-mannose-type Man5 (Fig. 1E). DSC was used to evaluate the thermal stability of IMM2520. The analysis revealed melting temperatures (Tm1 and Tm2) of 61.9 °C and 88.4 °C, respectively, signifying excellent stability of IMM2520 for accelerated stability testing in routine laboratory detection (Fig. 1F). The quality analysis

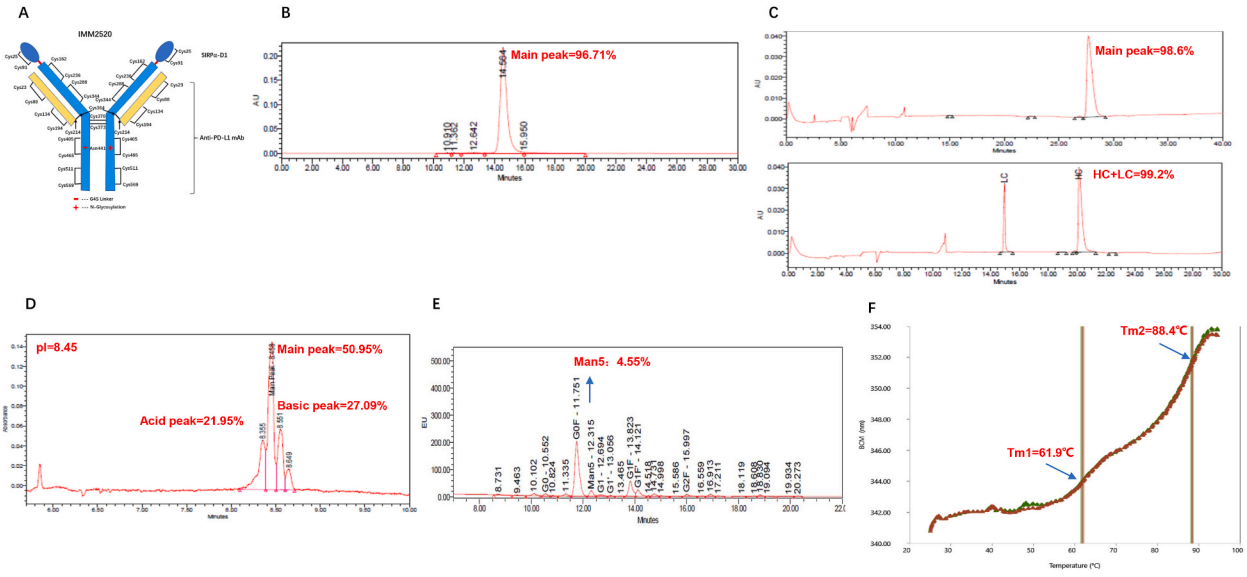

Fig. 1. Generation and quality analysis of IMM2520. (A) Structure diagram of IMM2520 bispecific antibody. (B) Polymer content of IMM2520 was analyzed using size exclusion chromatography-high performance liquid chromatography (SEC-HPLC). SEC-HPLC analysis indicated that the proportion of IMM2520 main peak was 96.71 %. There was no obvious polymer. (C) IMM2520 degradation was assessed through reductive capillary gel electrophoresis (rCE)-SDS and non-rCE (nrCE)-SDS analysis. The nrCE-SDS analysis confirmed that IMM2520 displayed no observable signs of degradation. The rCE-SDS analysis indicated that IMM2520 revealed no noticeable breakage in either chain. (D) Isoelectric point of IMM2520 was determined by imaging capillary isoelectric focusing electrophoresis (iCIEF) analysis. The isoelectric point of IMM2520 was 8.45, closely aligning with the theoretical value of pI = 8.39. (E) N-sugar-type analysis was conducted on IMM2520. IMM2520 displayed a typical IgG sugar type with no complex sialic acid modification and a slightly higher proportion of high-mannose-type Man5. (F) Differential scanning calorimetry was employed to determine the Tm value of IMM2520. The analysis revealed the excellent stability of IMM2520.

of IMM2520 indicated satisfactory purity and stability, meeting the quality requirements for antibody drug formulation.

3.2. Binding activity of IMM2520 to PD-L1 and CD47

The simultaneous targeting of hCD47and hPD-L1 by IMM2520 was validated by quantifying the affinities toward hPD-L1 and hCD47 using BLI. IMM2520 demonstrated an affinity for hCD47 at 2.49 nM (Fig. 2A) and for hPD-L1 at 0.576 nM (Fig. 2B).The binding affinity analysis reveals that IMM2520 exhibits a strong binding capacity to human and monkey PD-L1, while it does not exhibit any binding affinity towards mouse PD-L1. (Supplementary Figs. 1A–B). The interaction of IMM2520 with both hPD-L1 and hPD-L2 was examined, confirming specific binding only with hPD-L1 (Supplementary Fig. 1C). ELISA was utilized to assess IMM2520's binding activity to hPD-L1 and hCD47, comparing it with control groups consisting of IMM01 (SIRPα Fc fusion protein) and atezolizumab (an antibody against hPD-L1). The results showed IMM2520's median effective concentration (EC_{50}) for binding to hCD47 at 0.079 nM (Fig. 2C) and for binding to hPD-L1 at 0.456 nM (Fig. 2D). Subsequent confirmation through BLI analyses confirmed the ability of IMM2520 to simultaneously bind to both hPD-L1 and hCD47. Specifically, BLI measurements indicated that IMM2520, after initially binding to either hPD-L1 or hCD47, could subsequently bind to the other target (Fig. 2E).

3.3. IMM2520 disrupting both CD47/SIRPα and PD-1/PD-L1 interaction

The binding activity of IMM2520 with Jurkat and CHO-PD-L1 cells was assessed using flow cytometry. Positive controls included IMM01, atezolizumab, and IMM2515H. The results indicated significant binding of IMM2520 to Jurkat and CHO-PD-L1 cells, with EC_{50} values of 13.26 nM and 0.845 nM, respectively (Fig. 3A–B). By employing flow cytometry, the inhibitory potential of IMM2520 on the interaction between SIRPα and CD47 on tumor cell surfaces was assessed, revealing a substantial blocking effect on the binding of SIRPα to CD47 in both Jurkat cells ($CD47^{+}$/$PD\text{-}L1^{-}$) and RKO cells ($CD47^{+}$/$PD\text{-}L1^{+}$), with IC_{50} values of 64.08 nM and 0.01438 nM, respectively (Fig. 3C–D). In tumor cells expressing both PD-L1 and CD47, IMM2520's blocking efficacy on the CD47 target was notably higher than that of IMM01. Additionally, the capacity of IMM2520 to inhibit the interaction between PD-1 and PD-L1 on tumor cell surfaces was examined using flow cytometry, displaying significant inhibition of PD-1 binding to CHO-PD-L1 cells ($CD47^{-}$/$PD\text{-}L1^{+}$) and RKO cells ($CD47^{+}$/$PD\text{-}L1^{+}$), with IC_{50} values of 0.121 nM and 0.0123 nM, respectively (Fig. 3E–F). The inhibitory effect of

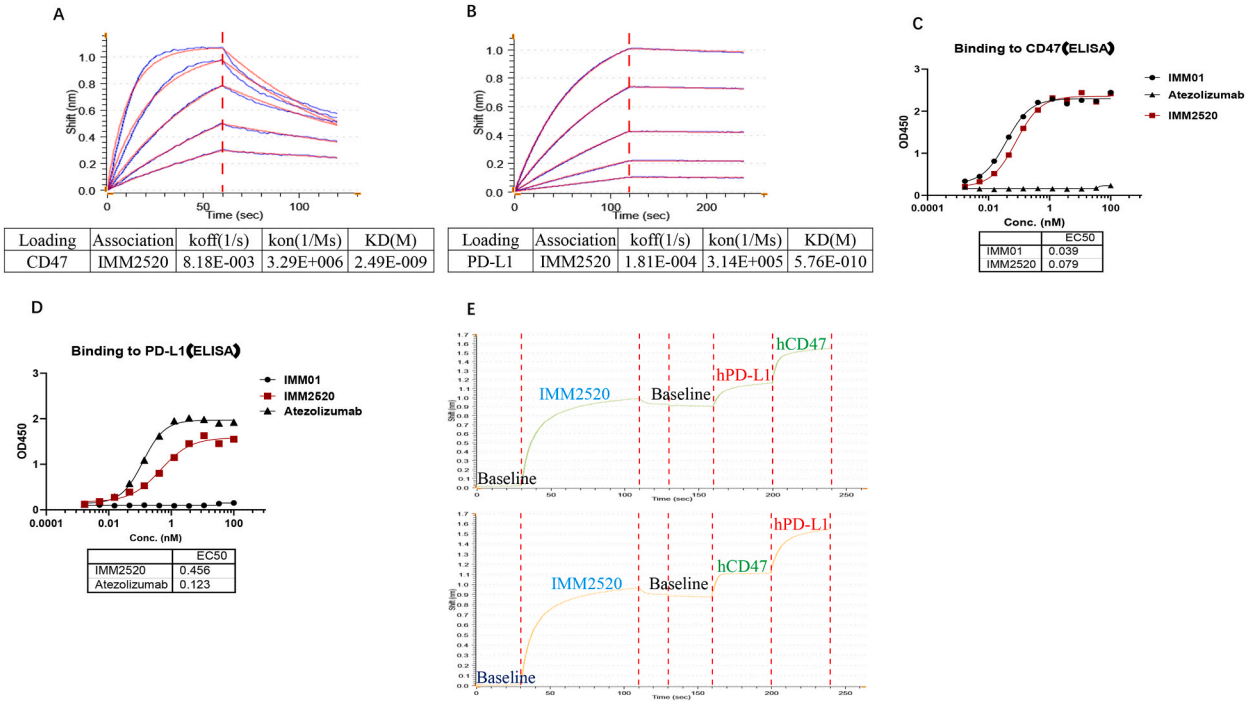

Loading	Association	koff(1/s)	kon(1/Ms)	KD(M)
CD47	IMM2520	8.18E-003	3.29E+006	2.49E-009

Loading	Association	koff(1/s)	kon(1/Ms)	KD(M)
PD-L1	IMM2520	1.81E-004	3.14E+005	5.76E-010

	EC50
IMM01	0.039
IMM2520	0.079

	EC50
IMM2520	0.456
Atezolizumab	0.123

Fig. 2. Binding activity of IMM2520 withCD47/PD-L1. (A) The affinity between IMM2520 and hCD47 was assessed using biolayer interferometry (BLI). The dissociation constant (KD) of IMM2520 to human CD47 was determined to be 2.49 nM. (B) The affinity between IMM2520 and hPD-L1 was assessed using BLI, and the KD value was 0.576 nM. (C) The binding activity of IMM2520 to hCD47 was assessed using enzyme-linked immunosorbent assay (ELISA). The EC_{50} of IMM2520 to hCD47 was 0.079 nM; IMM01 was the positive control of hCD47, and atezolizumab was the negative control. (D) The binding activity of IMM2520 to hPD-L1 was assessed by ELISA. The EC_{50} of IMM2520 to hPD-L1 was 0.456 nM. Atezolizumab was the positive control of hPD-L1, and IMM01 was the negative control. (E) Simultaneous binding of IMM2520 to purified hPD-L1 and hCD47 was measured by BLI. BLI measurements indicated that IMM2520, after initially binding to either hPD-L1 or hCD47, could subsequently bind to the other target.

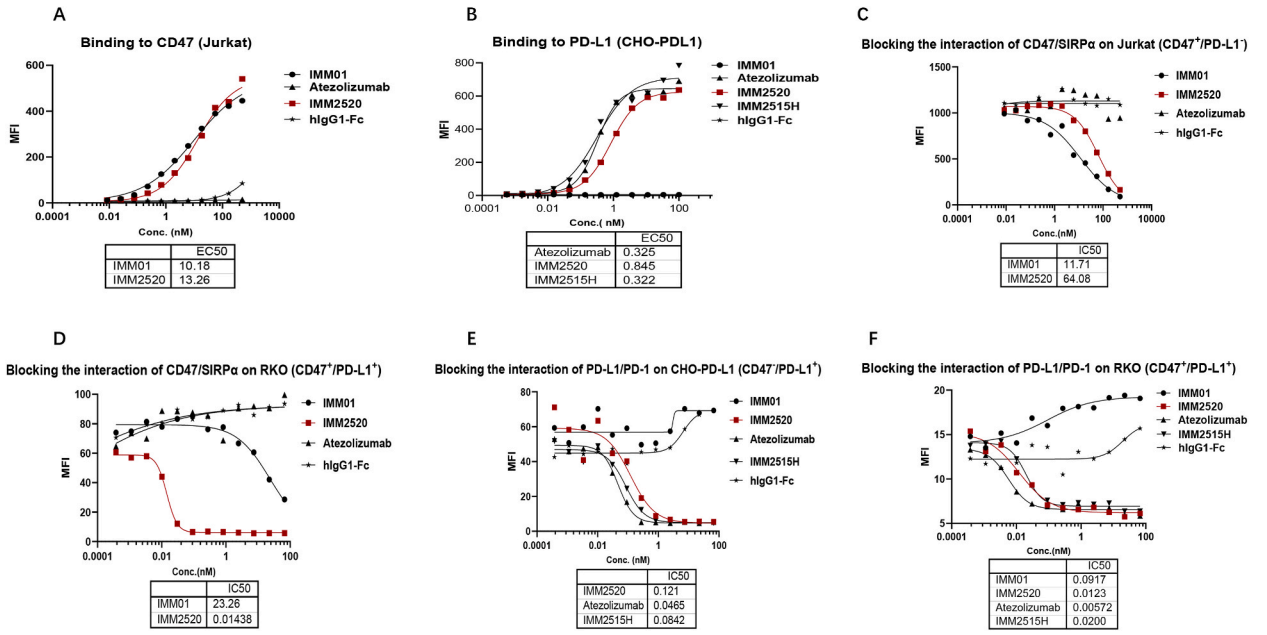

Fig. 3. IMM2520 blocking both CD47/SIRPα and PD-1/PD-L1 interaction. (A) IMM2520 bound to Jurkat cells. The EC_{50} of IMM2520 binding to Jurkat cells was 13.26 nM, and the binding ability was similar to that of IMM01. (B) IMM2520 bound to CHO-PD-L1 cells. The EC_{50} for IMM2520 binding to CHO-PD-L1 cells was 0.845 nM, and the binding ability was similar to that of atezolizumab and IMM2515H. (C) Interaction between CD47 and SIRPα was effectively inhibited by IMM2520 as demonstrated through flow cytometry analysis. IMM2520 could inhibit the binding of CD47 and SIRPα on Jurkat cells, with the IC_{50} value of 64.08 nM. This blocking activity was comparable to that of control IMM01. (D) Interaction between CD47 and SIRPα, which was blocked by IMM2520, was assessed by flow cytometry. IMM2520 effectively inhibited the binding of CD47 and SIRPα on RKO cells (PD-L1$^+$ and CD47$^+$ tumor cell), exhibiting superior blocking activity over the control IMM01 with the IC_{50} value of 0.01438 nM. (E) Interaction between PD-1 and PD-L1, which was inhibited by IMM2520, was evaluated by flow cytometry. IMM2520 demonstrated a significant inhibitory effect on the interaction between PD-1 and PD-L1 in CHO-PD-L1 cells, with an IC_{50} value of 0.121 nM. This blocking ability was equivalent to that of the control antibody atezolizumab and IMM2515H. (F) Flow cytometry analysis revealed that IMM2520 effectively blocked the interaction between PD-1 and PD-L1 on RKO cells. The IC_{50} value for this inhibition was determined as 0.0123 nM. The blocking activity was similar to that of the control antibody atezolizumab and IMM2515H.

IMM2520 on PD-1 was comparable to that of IMM2515H in tumor cells positive for CD47/PD-L1.

3.4. Enhanced antitumor efficacy of IMM2520 through ADCC and ADCP mechanism

The expression levels of PD-L1and CD47 were examined in RKO, ES-2, HT-1080, and HCC827 tumor cells to evaluate IMM2520's antitumor activity against double-positive tumor cells. The results revealed significantly increased levels of PD-L1and CD47 expression in all tumor cell lines (Fig. 4A). Additionally, the binding affinity of IMM2520 with PD-L1 and CD47 double-positive tumor cells was evaluated using flow cytometry. The outcomes demonstrated a substantial affinity between IMM2520 and tumor cells that are positive for both PD-L1 and CD47 (Fig. 4B–E). The primary objective behind designing IMM2520 was to provoke a durable tumor-specific immune response by targeting CD47 and PD-L1 on tumor cells, concurrently activating macrophages and T cells to achieve a synergistic effect. To ascertain the ADCC effect of IMM2520 attributed to the PD-L1 antibody, ADCC activity assessment was conducted using Raji cells and PD-L1 overexpressed Raji cells. The findings indicated selective cytotoxicity of IMM2520 against Raji-PD-L1 cells with an EC_{50} value of 1.842 pM, while no cytotoxicity was observed toward Raji cells (Fig. 5A). Furthermore, ADCC activity analysis was conducted on PD-L1and CD47 double-positive tumor cells (RKO, HCC827, HT-1080, and ES-2), revealing a significant ADCC effect of IMM2520 on these cell lines. The EC_{50} values for RKO, HCC827, HT-1080, and ES-2 cells were 1.440 pM, 4.678 pM, 7.196 pM, and 1.624 pM, respectively (Fig. 5B–E). The results demonstrated a significantly higher ADCC activity mediated by IMM2520 in tumor cells that were positive for both PD-L1 and CD47, compared to IMM2515H(ImmuneOnco, an antibody against hPD-L1). Investigation into the CDC effect of IMM2520 on Raji-PD-L1 cells showed no observable CDC effect (Supplementary Fig. 2). Additionally, the ADCP activity of IMM2520 against RKO, ES-2, HT-1080, and HCC827 cells was assessed. The results demonstrated that IMM2520 effectively stimulated THP-1 cells to phagocytose RKO, ES-2, HT-1080, and HCC827 cells, with calculated EC_{50} values of 0.006758 nM, 0.01034 nM, 0.007860 nM, and 0.01817 nM, respectively (Fig. 5F–I).

3.5. Safety assessment of IMM2520 in vitro

The current clinical studies have demonstrated that CD47 antibodies can effectively induce platelets aggregation and red blood

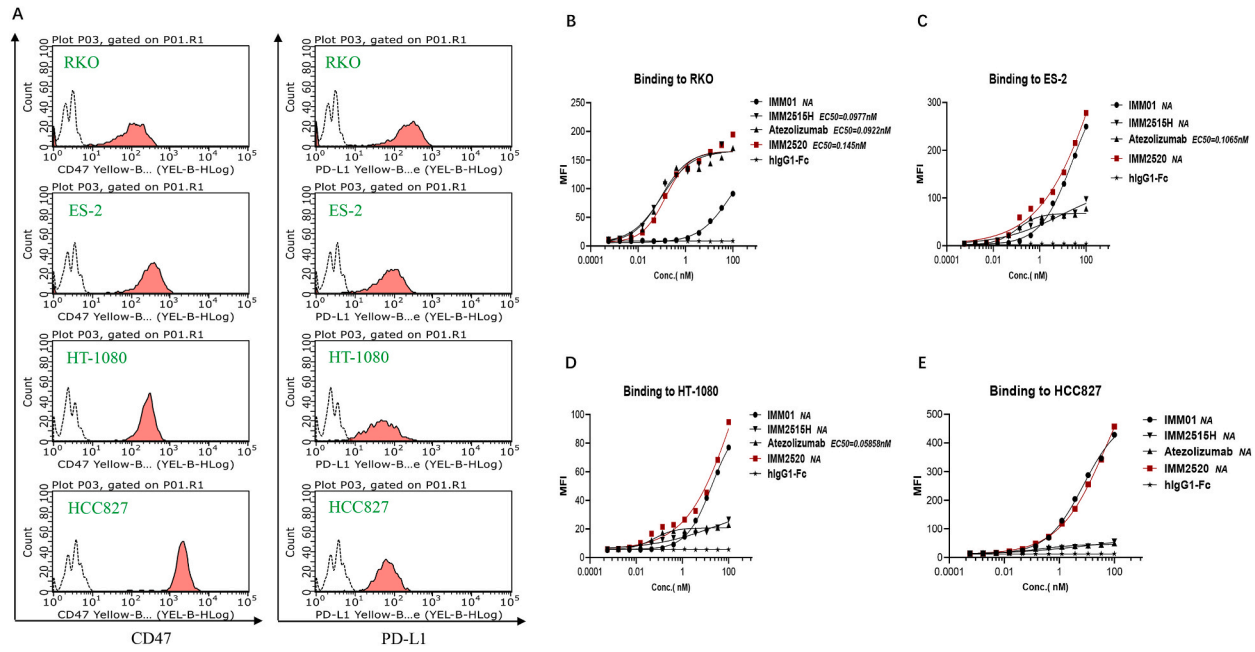

Fig. 4. IMM2520 binding to CD47/PD-L1 double-positive cells. (A) CD47 and PD-L1 expression in RKO, ES-2, HT-1080, and HCC827 cells was assessed by flow cytometry. The results revealed significantly levels of PD-L1 and CD47 expression in all tumor cell lines. (B), (C), (D), (E) Binding activity of IMM2520 with RKO, ES-2, HT-1080, and HCC827 cells was assessed by flow cytometry. The EC_{50} value for RKO was determined as 0.145 nM. The notation "NA" was that the calculation of EC_{50} had not been performed. hIgG1-Fc, IMM01, atezolizumab, and IMM2515H were employed as control antibodies.

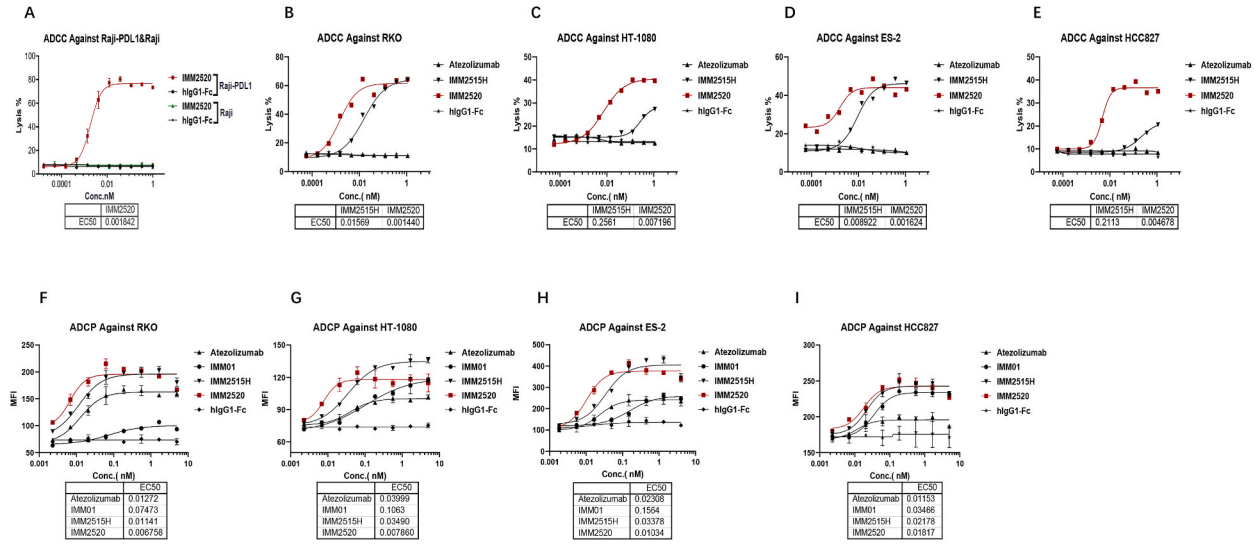

Fig. 5. Antitumor efficacy of IMM2520 *in vitro*. (A) Antibody-dependent cytotoxicity (ADCC) activities of Raji-PD-L1 and Raji cells were mediated by IMM2520. IMM2520 effectively regulates FcR-TANK cells to execute targeted antibody-dependent cytotoxicity against Raji-PD-L1, with the EC_{50} value of 1.842pM, but rather than Raji. (B), (C), (D), (E) ADCC activity of FcR-TANK cells against RKO, HCC827, ES-2, and HT-1080 cells was regulated by IMM2520, with EC_{50} values of 1.440 pM, 4.678 pM, 1.624 pM, and 7.196 pM, respectively. (F), (G), (H), (I) IMM2520 treatment significantly enhanced the phagocytic activity of THP-1 cells against RKO, HT-1080, ES-2, and HCC827 cells, with EC_{50} values of 0.006758 nM, 0.007860, 0.01034 nM, and 0.01817 nM, respectively.

cells agglutination [21,22]. The adverse effects are related to an upregulation of CD47 expression in red blood cells, particularly in aged erythrocytes. Inhibiting CD47 on these cells induces macrophage-mediated phagocytic clearance [31]. Therefore, prioritizing specific binding to $CD47^{+}$ tumor during the screening and optimization of CD47 candidate antibodies was crucial, aiming to avoid

binding to red blood cells. The binding of IMM2520 to human, cynomolgus monkey, rat, and mouse red blood cells was assessed using flow cytometry. The control groups included Hu-5F9 (anti-human CD47 monoclonal antibody), IMM01, atezolizumab, and IMM2515H. The results demonstrated that while IMM2520 did not exhibit binding affinity towards human, rat, and mouse red blood cells, it exhibited significant binding to monkey red blood cells (Fig. 6A, Supplementary Figs. 3A–C). Previous research results have shown that N-linked glycosylation of CD47 contributes to the non-binding characteristics of SIRPα-D1, as reflected by the recovery of red blood cell binding upon deglycosylation [29]. Furthermore, the binding of IMM2520 with human, cynomolgus monkey, rat, and mouse PBMCs was detected by flow cytometry. The findings revealed that IMM2520 did not bind to rat and mouse PBMCs but exhibited significant binding to human and monkey PBMCs, with EC_{50} values of 188.2 nM and 300.9 nM, respectively (Fig. 6B, Supplementary Figs. 3D–F). The binding of IMM2520 with human platelets was assessed using flow cytometry, revealing a robust interaction and an EC_{50} value of 4.897 μg/mL (Fig. 6C). The agglutination reaction between Hu-5F9 and human RBCs was visually observed, but no agglutination between IMM2520 and RBCs within the detected concentration range of 1000 nM–0.02 nM (Fig. 6D). The binding affinity of IMM2520 with mixed cells was analyzed using flow cytometry, including Raji and Raji-PD-L1, revealed a preference for binding of IMM2520 to Raji-PD-L1 cells over Raji cells (Fig. 6E). These findings suggest that IMM2520 exhibited preferential binding toward CD47 and PD-L1 double-positive tumor cells, indicating its reduced potential for off-target effects *in vivo* compared to CD47 therapeutic antibodies. Additionally, PBMCs from a healthy donor were used to evaluate the impact of IMM2520 on PBMC cytokine expression. The findings indicated that IMM2520 had no significant impact on the expression of IL-1β, IL-2, IL-4, IL-5, IL-10, GM-CSF, IFN-γ, and TNF-α. However, there was a notable upregulation in the expression of IL-6 (EC_{50} = 333.3 nM) and IL-8 (EC_{50} = 52.76 nM) in PBMCs (Fig. 6F). This result suggested that IMM2520 may induce cytokine storms in clinical studies, so relevant response strategies need to be developed before clinical trials.

3.6. Therapeutic effect of IMM2520 in vivo

To research the therapeutic effectiveness of IMM2520 *in vivo*, CT26-hPD-L1/hCD47 tumor cells were subcutaneously inoculated with humanized mice (BALB/c-hPD1/hSIRPα) on the 6th day post-inoculation. Different doses (0.3, 1, and 3 mg/kg) of IMM2520 and a control group treated with a diluent buffer were administered intraperitoneally. Tumor growth data were collected on the 19th day after treatment. The comparative analysis revealed that IMM2520 doses of 0.3 mg/kg (TGItv = 38.91 %) and 1 mg/kg (TGItv = 48.79 %) did not exhibit a significant inhibitory effect on tumor growth when compared to the control group. However, at a dose of 3 mg/kg (TGI_{tv} = 90.12 %), there was a notable suppression of tumor growth ($P < 0.01$; Fig. 7A–C). Throughout the treatment, following randomization, the body weight of mice in all treatment groups remained relatively stable without any noticeable bias or abnormalities (Fig. 7D).

In another model using CT26-hPD-L1/hCD47 syngeneic mice in BALB/c-hPD1/hSIRPα, on the 7th day post-transplantation, 6 mg/

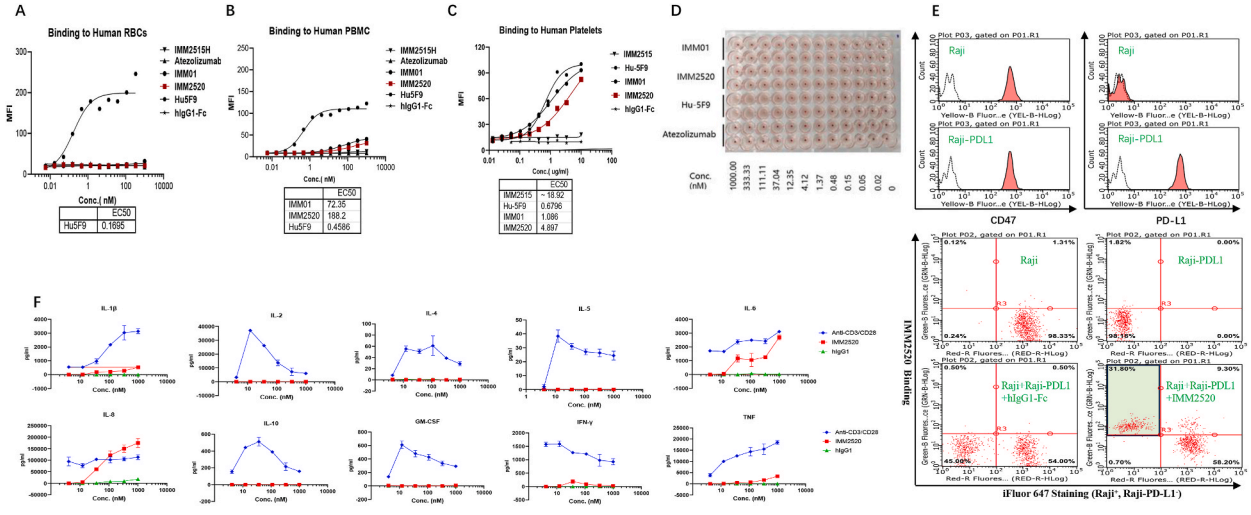

Fig. 6. Safety assessment of IMM2520 *in vitro*. (A) IMM2520 exhibited no binding affinity toward human red blood cells, whereas the control antibody Hu-5F9 demonstrated strong binding to human red blood cells. (B) Binding affinity between IMM2520 and human peripheral blood mononuclear cells (PBMCs) was evaluated by flow cytometry. The finding revealed that IMM2520 could bind to human PBMCs, with EC_{50} values of 188.2 nM. (C) The binding of IMM2520 to human platelets was assessed using flow cytometry, and the EC_{50} was 4.897 μg/mL(D) IMM2520 antibody concentration ranged from 1000 nM to 0.02 nM, and no erythrocyte agglutination was observed. (E) IMM2520 exhibited a tendency to selectively bind to cells that express both CD47 and PD-L1. Raji cells were stained with iFluor647 dye and subsequently co-cultured with Raji -PD-L1 cells at a 1:1 ratio. Subsequently, IMM2520 was diluted to 0.1 μg/mL for co-incubation with the aforementioned cell mixtures, while hIgG1-Fc was employed as the control group. The FITC-conjugated anti-human IgG (Fc) antibody was ultimately introduced and subsequently detected using flow cytometry. (F) IMM2520 administration led to significant upregulation in the expression of IL-6 (EC_{50} = 333.3 nM) and IL-8 (EC_{50} = 52.76 nM) in PBMCs.

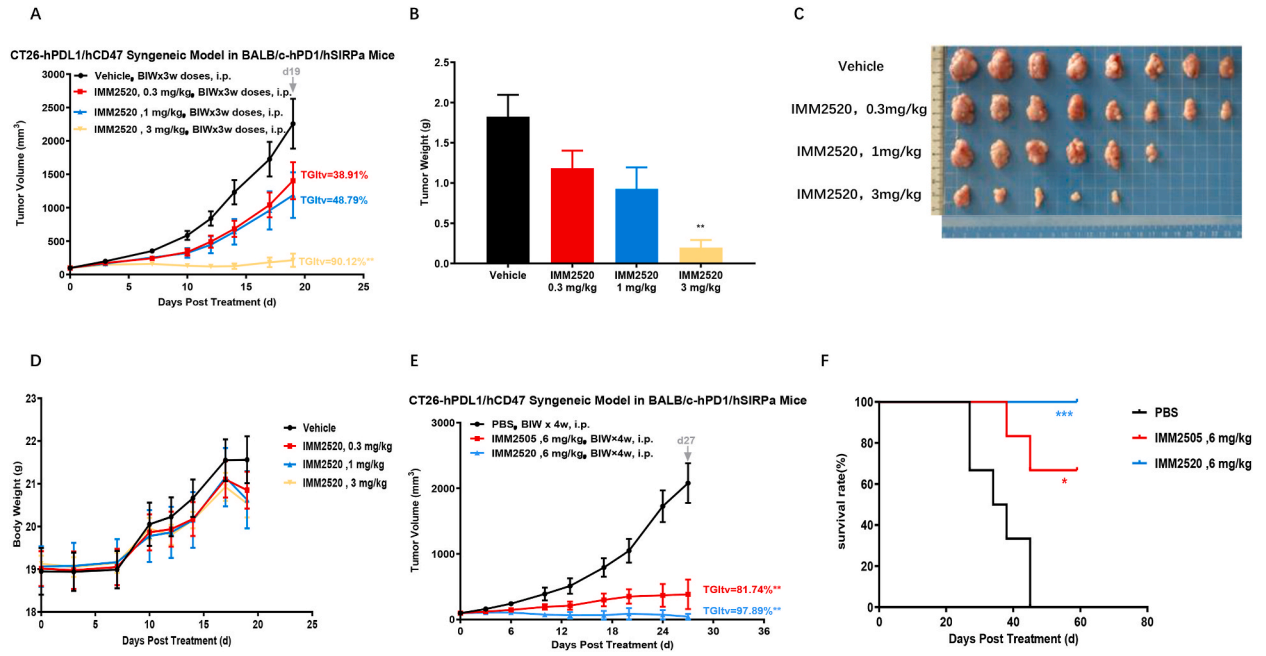

Fig. 7. *In vivo* efficacy of IMM2520 antitumor activity in transplanted mouse models. (A) Antitumor activity of IMM2520 exhibited a dose-dependent response. Notably, the tumor-killing efficacy was significantly enhanced at a dose of 3 mg/kg when compared with that at lower doses of 0.3 mg/kg and 1 mg/kg. (B) Tumor weight of IMM2520 on day 19 during treatment. Mean ± standard error of the mean was utilized to present the reported data, a two-factor analysis of variance was employed for determining significance, and the Tukey multiple comparison test was conducted for comparison with the diluent control group. "*" $p < 0.05$; "**" $p < 0.01$, and "***" $p < 0.001$. (C) Tumor images at the endpoint of the experiment. (D) Body weight of mice remained consistent throughout the IMM2520 treatment. (E) Tumor-killing efficacy of IMM2520 exhibited greater potency than that of IMM2505. Compared with the PBS control group, IMM2505 (6 mg/kg) exhibited a tumor inhibition rate (TGI_{tv}) of 81.74 %, whereas IMM2520 (6 mg/kg) showed a TGI_{tv} of 97.89 %. (F)The Kaplan-Meier survival curve of CT26-hPD-L1/hCD47 transplanted mice was analyzed following IMM2520 treatment. The survival rate of mice treated with IMM2520 (6 mg/kg) was higher than that of IMM2505-treated mice.

kg of IMM2505 (based on atezolizumab backbone), 6 mg/kg of IMM2520, and a control group treated with PBS were intraperitoneally administered after randomly grouped based on tumor volume. Statistical analysis of tumor growth data was conducted on the 27th day post-administration. Compared with the PBS control group, IMM2505 (6 mg/kg) exhibited a tumor inhibition rate (TGI_{tv}) of 81.74 %, whereas IMM2520 (6 mg/kg) showed a TGI_{tv} of 97.89 %. Both compounds demonstrated significant inhibitory effects on tumor growth ($P < 0.01$; Fig. 7E). Additionally, the survival rate of mice treated with IMM2505 (6 mg/kg) showed a significant enhancement in comparison to the PBS control group ($P < 0.05$). Moreover, the survival rate of mice treated with IMM2520 (6 mg/kg) was even higher than that of IMM2505-treated mice and significantly improved compared to the PBS control group ($P < 0.001$; Fig. 7F).

MC38-hCD47/hPD-L1 colon cancer cells were subcutaneously inoculated into C57BL/6J-hPD-1/hSIRPα/hCD47 mice, and thereafter grouped randomly based on tumor volume on day 6 post-inoculation. Intravenous administration of vehicle and IMM2520 occurred at different doses (2 mg/kg, 6 mg/kg, 20 mg/kg). Comparative analysis revealed that IMM2520 exhibited a significant dose-dependent inhibitory effect on tumor growth at doses of 2 mg/kg ($TGI_{tv} = 49.32$ %, $P < 0.05$), 6 mg/kg ($TGI_{tv} = 69.83$ %, $P < 0.01$), and 20 mg/kg ($TGI_{tv} = 84.47$ %, $P < 0.01$) compared to the control group (Supplementary Figs. 4A–B).

4. Discussion

The U.S. Food and Drug Administration has granted approval for a range of PD-1 or PD-L1 inhibitors, thereby expanding the accessibility of these drugs for diverse therapeutic applications The efficacy rate of monotherapy with PD-1/PD-L1 antibody drugs for certain solid tumors ranges from 30 % to 45 % [32,33]. Additionally, combining PD-1 or PD-L1 antibody drugs with other drugs in the management of lung cancer, melanoma, and kidney cancer can achieve a maximum remission rate of approximately 50 % [34–36]. However, a subset of patients receiving treatment with ICIs may develop primary or acquired resistance to the tumor following initial therapy. The most used approach to address primary resistance involves developing combination therapies targeting multiple targets simultaneously.

The signaling pathway of PD-1 and its ligand PD-L1 plays a crucial role in acquired immunity primarily due to the expression of PD-1 on activated T cells [25]. In the tumor microenvironment, both tumor cells and tumor-associated antigen-presenting cells (APCs) exhibit elevated expression of PD-L1,while tumor-infiltrating lymphocytes exhibit increased PD-1 expression due to prolonged stimulation by tumor antigens. The PD-L1/PD-1 pathway suppresses the effector function of antigen-specific $CD8^+$ T cells by

regulating T cell apoptosis, dysfunction, and exhaustion, while facilitating tumor immune evasion [37,38]. The previous study has demonstrated that CD47/PD-L1 dual antibody treatment in mouse tumor models leads to a significant augmentation in the population of $CD8^+$ T cells within the tumor microenvironment, concomitant with a notable reduction in Treg-associated cells. Furthermore, this dual antibody therapy also induces a substantial upregulation of CXCL9, CXCL 10, and CCL5 chemokines responsible for recruiting $CD8^+$ T cells to tumor sites [39]. The *in vitro* activity analysis demonstrated the potent inhibitory effect of IMM2520 on the interaction between PD-1 and PD-L1. The blocking and binding activities of IMM2520 against the PD-L1 target were comparable to the corresponding monoclonal antibody. The administration of IMM2520 effectively abrogated the PD-L1-mediated immunosuppressive signaling pathway in cancer cells, thereby potentiating T cell activation within the tumor microenvironment, eliciting cytokine release, and ultimately accomplishing the objective of efficient tumor eradication. Additionally, the efficacy of IMM2520 is further enhanced by leveraging the regulatory capabilities of antibody Fc, such as ADCC or ADCP, to exert direct cytotoxic effects on tumors (Fig. 8).

The expression of CD47 is markedly elevated in various hematologic malignancies and solid tumors, exerting inhibitory effects on the innate immune function of myeloid-derived immune cells [40–42]. A plethora of studies have unequivocally demonstrated the pivotal role of the CD47/SIRPα signaling pathway in mediating macrophage phagocytosis and facilitating tumor antigen presentation [39,43]. CD47 expression by tumor confers protection from macrophage-mediated phagocytosis, aiding in the evasion of immune responses. The enhancement of tumor phagocytosis by macrophages is achieved through the inhibition of CD47 and SIRPα signaling pathways. The presentation of tumor antigens to T cells by macrophages occurs via major histocompatibility complex I, thereby triggering the activation of $CD8^+$ T cells that possess the ability to selectively target and eliminate tumors [44]. The analysis results indicated that IMM2520 effectively bound to CD47 on the tumor and inhibited the binding of CD47-SIRPα, thereby promoting macrophage-mediated phagocytosis of the tumor (Fig. 8). Notably, RBCs also highly expressed CD47, acting as a "do not eat me" signal to evade macrophage clearance [45]. An ideal therapeutic drug targeting CD47 should selectively prompt macrophages to engulf tumor cells, activate T cells, and avoid binding to RBCs. Compared with existing CD47-targeted therapies, IMM2520, engineered to target CD47 through SIRPα, selectively binds to tumor cells' CD47 while avoiding interactions with CD47 expressed on RBCs. Unlike other antibodies targeting CD47 or CD47/PD-L1, IMM2520 demonstrates no binding affinity toward human RBCs, even at high concentrations, potentially offering a safety profile in preclinical and subsequent human clinical trials.

First-generation CD47-targeting drugs such as CD47 monoclonal antibodies [46,47] and SIRPα fusion proteins [48,49] are presently in clinical trials, primarily for hematological malignancies, showing moderate antitumor activity to these tumor types. Currently, CD47-targeted therapies are primarily combined with other antitumor agents to augment the efficacy of CD47 antibodies [46,49,50]. A rational combination of targeting both innate and adaptive checkpoints, particularly when used in conjunction with other ICIs, can significantly enhance therapeutic effectiveness [23,51–53]. Currently, there are also studies being reported about CD47/PD-L1 bispecific antibodies. For example, the IBI322 is structured as "1 + 2″ and is generated through the knobs-into-holes strategy. The CD47 arm comprises an antibody Fab, while the PD-L1 arm consists of two tandem single-domain antibodies (VHH) connected by amino acid linker (G4S) [39]. The bispecific antibody 6MW3211 is designed in the IgG4 format, utilizing the in-hole knob (KIH) technique, and possesses a common light chain architecture. The knob arm corresponds to the CD47 antibody heavy chain, and the hole arm corresponds to the PD-L1 antibody heavy chain [25]. The αCD47/PD-L1 antibody is a fully human IgG1 type that utilizes the knobs-in-holes technique and features a common light chain structure. It exhibits moderate affinity towards CD47 and high affinity towards PD-L1 [53]. HX009 is a bispecific antibody with a "2 × 2″ symmetric structure, consisting of the extracellular CD47 binding domain of human SIRP alpha protein fused to the Fc end of PD1 antibody. This design ensures high affinity binding to PD1 while significantly reducing its affinity for CD47 [54]. Therefore, IMM2520 is specifically designed to synergistically reshape the tumor microenvironment by targeting both innate and adaptive immune checkpoints, thereby enhancing potent antitumor activity.

IMM2520 exhibits higher affinity toward PD-L1 on tumor cells, whereas SIRPα demonstrated a relatively lower affinity for CD47 on tumor cells. Despite its low affinity with CD47, IMM2520 effectively stimulates macrophages to phagocytose tumor cells. When IMM2520 binds to PD-L1 on cancer cells, it enhances the affinity of its binding to SIRPα, obstructs the binding of CD47 to SIRPα, and effectively inhibits tumor progression. IMM2520 also demonstrated significantly higher IMM2520-mediated ADCC activity in PD-L1 and CD47 double-positive tumor cells than PD-L1 monoclonal antibody. Additionally, IMM2520 exhibits a preferential binding affinity towards tumor cells that express both PD-L1 and CD47 in the tumor microenvironment, thus, effectively reducing off-target effects associated with the CD47 arm. In a hPD1/hSIRPα transgenic mouse model, IMM2520 effectively inhibited tumor growth owing to its antitumor effects. The US Food and Drug Administration and China National Medical Products Administration have approved the clinical application of IMM2520, and ongoing clinical trials (NCT05780307, CTR20230255) are evaluating its efficacy and safety in human patients. We have initiated the Phase I study of IMM2520 targeting various advanced solid tumors and dosed the first patient in March 2023. By the end of 2023, 12 patients in total have been enrolled and dosed. The preliminary data suggests that IMM2520 demonstrates a favorable safety profile and is well tolerated, with no significant adverse effects observed, even at doses up to 3.0 mg/kg. The dose escalation is still ongoing. Three stable diseases (SDs) with tumor shrinkage over 10 % were achieved for a patient with cervical cancer at 0.1 mg/kg, a patient with small cell lung cancer (SCLC) and a patient with colorectal cancer at 2.0 mg/kg. Among them, one SCLC patient who progressed after PD-1 antibody treatment has achieved tumor shrinkage of 26.3 % after 4 cycles of treatment in January 2024.

5. Conclusions

The present study elucidates the development of IMM2520 antibody, which demonstrates remarkable specificity towards CD47 and PD-L1. Given the multiple mechanisms of action and unique design, IMM2520 concurrently engages both innate and adaptive immunity, modulates the immune function within the tumor microenvironment, suppresses tumor immune evasion, stimulates tumor cell

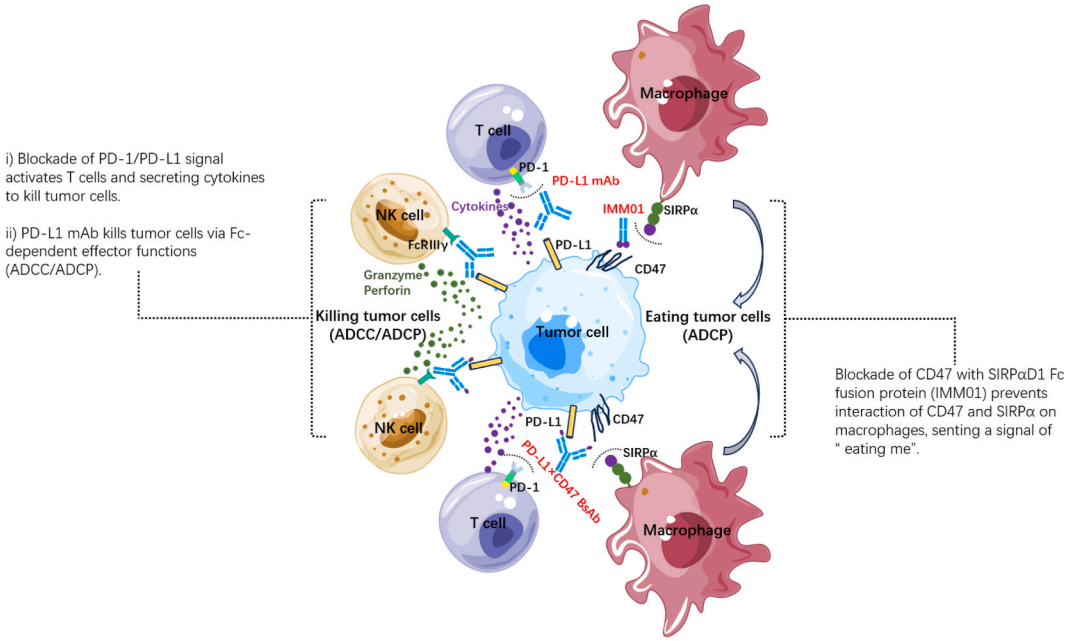

Fig. 8. Mechanism of action of IMM2520. The binding of IMM2520 to PD-L1 on the surfaces of tumor cells inhibits the signaling pathway of PD-1/PD-L1, thereby enhancing T-cell activation and cytokine secretion. Additionally, IMM2520 induces tumor cell death through the Fc-dependent effect function (antibody-dependent cytotoxicity and antibody-dependent phagocytosis) of PD-L1 antibody. Simultaneously, IMM2520 disrupts the interaction of CD47/SIRPα on macrophages, triggering an "eat me" signal that further activates macrophage immune responses and elicits a comprehensive immune reaction.

cytotoxicity, and demonstrates favorable hematotoxicity characteristics.

6. Limitations of the study

The limitations of this study include the utilization of cancer cell lines for *in vitro* investigations and transgenic mice for *in vivo* investigations, respectively. However, the authors selected a range of cancer cell lines (including RKO, ES-2, HT-1080 and HCC827) based on their expression profile of PD-L1 and CD47, which rendered them suitable candidates for investigation (Fig. 4A). In recent years, the stable integration of exogenous genes into the mouse genome has emerged as a highly effective strategy for various aspects of biological research. The author selected two transgenic models and repeatedly validated the strong antitumor activity of IMM2520 (Fig. 7A–F, Supplementary Figs. 4A–B). Simultaneously targeting PD-1/PD-L1 and CD47/SIRPα pathway provides a promising solution for cancer treatment. The therapeutic efficacy of blocking the PD-1/PD-L1 and CD47/SIRPα signaling has been demonstrated in numerous studies for the treatment of various types of cancers [39]. The affinity, binding, blocking, Fc-dependent effector functions, safety, and antitumor activity characteristics of IMM2520 were assessed through a range of *in vitro* and *in vivo* assays. The authors have initiated the Phase I study of IMM2520. The preliminary data has demonstrated that IMM2520 is safe, effective, and well tolerated up to 3.0 mg/kg. The dose escalation is still ongoing.

CRediT authorship contribution statement

Chunmei Yang: Writing – review & editing, Writing – original draft, Methodology, Investigation. **Song Li:** Writing – review & editing, Writing – original draft, Project administration, Methodology, Investigation, Conceptualization. **Dianze Chen:** Writing – review & editing, Software, Methodology, Investigation, Data curation. **Dandan Liu:** Writing – review & editing, Visualization, Validation. **Yanan Yang:** Writing – review & editing, Visualization, Validation. **Huiqin Guo:** Writing – review & editing, Visualization, Validation. **Nana Sun:** Writing – review & editing, Visualization, Validation. **Xing Bai:** Writing – review & editing, Visualization, Validation. **Guanghui Li:** Writing – review & editing, Visualization, Validation. **Ruliang Zhang:** Writing – review & editing, Visualization, Validation. **Tianxiang Wang:** Writing – review & editing, Visualization, Validation. **Li Zhang:** Writing – review & editing, Visualization, Validation. **Liang Peng:** Writing – review & editing, Visualization, Validation. **Sijin Liu:** Writing – review & editing, Visualization, Validation. **Wei Zhang:** Writing – review & editing, Visualization, Validation. **Gui Zhao:** Writing – review & editing, Visualization, Validation. **Xiaoping Tu:** Writing – review & editing, Visualization, Validation. **Wenzhi Tian:** Writing – review & editing, Project administration, Funding acquisition, Conceptualization.

Ethics approval and consent to participate

The animal study was reviewed and approved by the Institutional Animal Care and Use Committee (IACUC) of Gempharmatech Inc. (GPTAP20201125-3/GPTAP20211021-2) and Shanghai Model Organisms Center Inc. (2020-0047).

Consent for publication

Not applicable.

Data availability statement

All data generated and analyzed during this study are included in this article and supplementary file.

Funding

This study is funded by Immuneonco Biopharmaceuticals (Shanghai) Inc. Grant/award number is not applicable.

Declaration of competing interest

The authors declare the following financial interests/personal relationships which may be considered as potential competing interests:Wenzhi Tian and Song Li hold ownership interest (including patents) in ImmuneOnco Biopharmaceuticals (Shanghai) Inc. If there are other authors, they declare that they have no known competing financial interests or personal relationships that could have appeared to influence the work reported in this paper.

Acknowledgements

We would like to thank Gempharmatech Inc. and Shanghai Model Organisms Center Inc. for their wonderful services and technical support in the evaluation of *in vivo* efficacy.

Appendix A. Supplementary data

Supplementary data to this article can be found online at https://doi.org/10.1016/j.heliyon.2024.e39858.

References

[1] F. Bray, M. Laversanne, H. Sung, J. Ferlay, R.L. Siegel, I. Soerjomataram, A. Jemal, Global cancer statistics 2022: GLOBOCAN estimates of incidence and mortality worldwide for 36 cancers in 185 countries, CA Cancer J. Clin. 74 (3) (2024) 229–263, https://doi.org/10.3322/caac.21834.
[2] J.B. Swann, M.J. Smyth, Immune surveillance of tumors, J. Clin. Invest. 117 (5) (2007) 1137–1146, https://doi.org/10.1172/jci31405.
[3] R.D. Schreiber, L.J. Old, M.J. Smyth, Cancer immunoediting: integrating immunity's roles in cancer suppression and promotion, Science 331 (6024) (2011) 1565–1570, https://doi.org/10.1126/science.1203486.
[4] A. Makkouk, G.J. Weiner, Cancer immunotherapy and breaking immune tolerance: new approaches to an old challenge, Cancer Res. 75 (1) (2015) 5–10, https://doi.org/10.1158/0008-5472.Can-14-2538.
[5] C. Sun, R. Mezzadra, T.N. Schumacher, Regulation and function of the PD-L1 checkpoint, Immunity 48 (3) (2018) 434–452, https://doi.org/10.1016/j.immuni.2018.03.014.
[6] Q. Lei, D. Wang, K. Sun, L. Wang, Y. Zhang, Resistance mechanisms of anti-PD1/PDL1 therapy in solid tumors, Front. Cell Dev. Biol. 8 (2020) 672, https://doi.org/10.3389/fcell.2020.00672.
[7] C. Ghosh, G. Luong, Y. Sun, A snapshot of the PD-1/PD-L1 pathway, J. Cancer 12 (9) (2021) 2735–2746, https://doi.org/10.7150/jca.57334.
[8] L. Nayak, F.M. Iwamoto, A. LaCasce, S. Mukundan, M.G.M. Roemer, B. Chapuy, P. Armand, S.J. Rodig, M.A. Shipp, PD-1 blockade with nivolumab in relapsed/refractory primary central nervous system and testicular lymphoma, Blood 129 (23) (2017) 3071–3073, https://doi.org/10.1182/blood-2017-01-764209.
[9] S.M. Ansell, A.M. Lesokhin, I. Borrello, A. Halwani, E.C. Scott, M. Gutierrez, S.J. Schuster, M.M. Millenson, D. Cattry, G.J. Freeman, S.J. Rodig, B. Chapuy, A. H. Ligon, L. Zhu, J.F. Grosso, S.Y. Kim, J.M. Timmerman, M.A. Shipp, P. Armand, PD-1 blockade with nivolumab in relapsed or refractory Hodgkin's lymphoma, N. Engl. J. Med. 372 (4) (2015) 311–319, https://doi.org/10.1056/NEJMoa1411087.
[10] N. Tomioka, M. Azuma, M. Ikarashi, M. Yamamoto, M. Sato, K.I. Watanabe, K. Yamashiro, M. Takahashi, The therapeutic candidate for immune checkpoint inhibitors elucidated by the status of tumor-infiltrating lymphocytes (TILs) and programmed death ligand 1 (PD-L1) expression in triple negative breast cancer (TNBC), Breast Cancer 25 (1) (2018) 34–42, https://doi.org/10.1007/s12282-017-0781-0.
[11] R.S. Finn, S. Qin, M. Ikeda, P.R. Galle, M. Ducreux, T.Y. Kim, M. Kudo, V. Breder, P. Merle, A.O. Kaseb, D. Li, W. Verret, D.Z. Xu, S. Hernandez, J. Liu, C. Huang, S. Mulla, Y. Wang, H.Y. Lim, A.X. Zhu, A.L. Cheng, Atezolizumab plus Bevacizumab in unresectable hepatocellular carcinoma, N. Engl. J. Med. 382 (20) (2020) 1894–1905, https://doi.org/10.1056/NEJMoa1915745.
[12] T. Yau, Y.K. Kang, T.Y. Kim, A.B. El-Khoueiry, A. Santoro, B. Sangro, I. Melero, M. Kudo, M.M. Hou, A. Matilla, F. Tovoli, J.J. Knox, A. Ruth He, B.F. El-Rayes, M. Acosta-Rivera, H.Y. Lim, J. Neely, Y. Shen, T. Wisniewski, J. Anderson, C. Hsu, Efficacy and safety of nivolumab plus ipilimumab in patients with advanced hepatocellular Carcinoma previously treated with Sorafenib: the CheckMate 040 randomized clinical trial, JAMA Oncol. 6 (11) (2020) e204564, https://doi.org/10.1001/jamaoncol.2020.4564.
[13] B. Zhang, Q. Wu, Y.L. Zhou, X. Guo, J. Ge, J. Fu, Immune-related adverse events from combination immunotherapy in cancer patients: a comprehensive meta-analysis of randomized controlled trials, Int. Immunopharm. 63 (2018) 292–298, https://doi.org/10.1016/j.intimp.2018.08.014.
[14] C.F. Friedman, T.A. Proverbs-Singh, M.A. Postow, Treatment of the immune-related adverse effects of immune checkpoint inhibitors: a review, JAMA Oncol. 2 (10) (2016) 1346–1353, https://doi.org/10.1001/jamaoncol.2016.1051.

[15] Y. Sun, X. Yu, X. Wang, K. Yuan, G. Wang, L. Hu, G. Zhang, W. Pei, L. Wang, C. Sun, P. Yang, Bispecific antibodies in cancer therapy: target selection and regulatory requirements, Acta Pharm. Sin. B 13 (9) (2023) 3583–3597, https://doi.org/10.1016/j.apsb.2023.05.023.

[16] E. Dahlén, N. Veitonmäki, P. Norlén, Bispecific antibodies in cancer immunotherapy, Ther. Adv. Vaccines Immunother. 6 (1) (2018) 3–17, https://doi.org/10.1177/2515135518763280.

[17] M.E.W. Logtenberg, F.A. Scheeren, T.N. Schumacher, The CD47-SIRPα immune checkpoint, Immunity 52 (5) (2020) 742–752, https://doi.org/10.1016/j.immuni.2020.04.011.

[18] A. Veillette, J. Chen, SIRPα-CD47 immune checkpoint blockade in anticancer therapy, Trends Immunol. 39 (3) (2018) 173–184, https://doi.org/10.1016/j.it.2017.12.005.

[19] I. Mouro-Chanteloup, J. Delaunay, P. Gane, V. Nicolas, M. Johansen, E.J. Brown, L.L. Peters, C.L. Van Kim, J.P. Cartron, Y. Colin, Evidence that the red cell skeleton protein 4.2 interacts with the Rh membrane complex member CD47, Blood 101 (1) (2003) 338–344, https://doi.org/10.1182/blood-2002-04-1285.

[20] M. Olsson, P. Bruhns, W.A. Frazier, J.V. Ravetch, P.A. Oldenborg, Platelet homeostasis is regulated by platelet expression of CD47 under normal conditions and in passive immune thrombocytopenia, Blood 105 (9) (2005) 3577–3582, https://doi.org/10.1182/blood-2004-08-2980.

[21] B.I. Sikic, N. Lakhani, A. Patnaik, S.A. Shah, S.R. Chandana, D. Rasco, A.D. Colevas, T. O'Rourke, S. Narayanan, K. Papadopoulos, G.A. Fisher, V. Villalobos, S. S. Prohaska, M. Howard, M. Beeram, M.P. Chao, B. Agoram, J.Y. Chen, J. Huang, M. Axt, J. Liu, J.P. Volkmer, R. Majeti, I.L. Weissman, C.H. Takimoto, D. Supan, H.A. Wakelee, R. Aoki, M.D. Pegram, S.K. Padda, First-in-Human, first-in-class phase I trial of the anti-CD47 antibody Hu5F9-G4 in patients with advanced cancers, J. Clin. Oncol. 37 (12) (2019) 946–953, https://doi.org/10.1200/jco.18.02018.

[22] A.M. Zeidan, D.J. DeAngelo, J. Palmer, C.S. Seet, M.S. Tallman, X. Wei, H. Raymon, P. Sriraman, S. Kopytek, J.P. Bewersdorf, M.R. Burgess, K. Hege, W. Stock, Phase 1 study of anti-CD47 monoclonal antibody CC-90002 in patients with relapsed/refractory acute myeloid leukemia and high-risk myelodysplastic syndromes, Ann. Hematol. 101 (3) (2022) 557–569, https://doi.org/10.1007/s00277-021-04734-2.

[23] A. Zhang, Z. Ren, K.F. Tseng, X. Liu, H. Li, C. Lu, Y. Cai, J.D. Minna, Y.X. Fu, Dual targeting of CTLA-4 and CD47 on T(reg) cells promotes immunity against solid tumors, Sci. Transl. Med. 13 (605) (2021), https://doi.org/10.1126/scitranslmed.abg8693.

[24] M. Feng, W. Jiang, B.Y.S. Kim, C.C. Zhang, Y.X. Fu, I.L. Weissman, Phagocytosis checkpoints as new targets for cancer immunotherapy, Nat. Rev. Cancer 19 (10) (2019) 568–586, https://doi.org/10.1038/s41568-019-0183-z.

[25] R. Wang, C. Zhang, Y. Cao, J. Wang, S. Jiao, J. Zhang, M. Wang, P. Tang, Z. Ouyang, W. Liang, Y. Mao, A. Wang, G. Li, J. Zhang, M. Wang, S. Wang, X. Gui, Blockade of dual immune checkpoint inhibitory signals with a CD47/PD-L1 bispecific antibody for cancer treatment, Theranostics 13 (1) (2023) 148–160, https://doi.org/10.7150/thno.79367.

[26] H. Zhang, J. Yu, L.I. He, W. Qian, X. Xiao, Q. Cai, Y. Liu, Y. Zhang, L. Zhang, L. Qin, S216: CD47/PD-L1 bispecific antibody (IBI322) in anti-PD-1 or PD-L1 treatment-resistant classical Hodgkin lymphoma: a phase I study, HemaSphere 7 (2023) e8102841.

[27] Y.F. Zhang, Y. Sun, J. Hong, M. Ho, Humanization of the shark V(NAR) single domain antibody using CDR grafting, Curr. Protoc. 3 (1) (2023) e630, https://doi.org/10.1002/cpz1.630.

[28] J. Yu, S. Li, D. Chen, D. Liu, H. Guo, C. Yang, W. Zhang, L. Zhang, G. Zhao, X. Tu, L. Peng, S. Liu, X. Bai, Y. Song, Z. Jiang, R. Zhang, W. Tian, Crystal structure of human CD47 in complex with engineered SIRPα.D1(N80A), Molecules 27 (17) (2022) 5574, https://doi.org/10.3390/molecules27175574.

[29] J. Yu, S. Li, D. Chen, D. Liu, H. Guo, C. Yang, W. Zhang, L. Zhang, G. Zhao, X. Tu, L. Peng, S. Liu, X. Bai, Y. Song, Z. Jiang, R. Zhang, W. Tian, SIRPα-Fc fusion protein IMM01 exhibits dual anti-tumor activities by targeting CD47/SIRPα signal pathway via blocking the "don't eat me" signal and activating the "eat me" signal, J. Hematol. Oncol. 15 (1) (2022) 167, https://doi.org/10.1186/s13045-022-01385-2.

[30] R.L. Shields, A.K. Namenuk, K. Hong, Y.G. Meng, J. Rae, J. Briggs, D. Xie, J. Lai, A. Stadlen, B. Li, J.A. Fox, L.G. Presta, High resolution mapping of the binding site on human IgG1 for Fc gamma RI, Fc gamma RII, Fc gamma RIII, and FcRn and design of IgG1 variants with improved binding to the Fc gamma R, J. Biol. Chem. 276 (9) (2001) 6591–6604, https://doi.org/10.1074/jbc.M009483200.

[31] J. Liu, L. Wang, F. Zhao, S. Tseng, C. Narayanan, L. Shura, S. Willingham, M. Howard, S. Prohaska, J. Volkmer, M. Chao, I.L. Weissman, R. Majeti, Pre-clinical development of a humanized anti-CD47 antibody with anti-cancer therapeutic potential, PLoS One 10 (9) (2015) e0137345, https://doi.org/10.1371/journal.pone.0137345.

[32] C. Robert, J. Schachter, G.V. Long, A. Arance, J.J. Grob, L. Mortier, A. Daud, M.S. Carlino, C. McNeil, M. Lotem, J. Larkin, P. Lorigan, B. Neyns, C.U. Blank, O. Hamid, C. Mateus, R. Shapira-Frommer, M. Kosh, H. Zhou, N. Ibrahim, S. Ebbinghaus, A. Ribas, Pembrolizumab versus ipilimumab in advanced melanoma, N. Engl. J. Med. 372 (26) (2015) 2521–2532, https://doi.org/10.1056/NEJMoa1503093.

[33] D.F. McDermott, J.L. Lee, M. Ziobro, C. Suarez, P. Langiewicz, V.B. Matveev, P. Wiechno, R.A. Gafanov, P. Tomczak, F. Pouliot, F. Donskov, B.Y. Alekseev, S. J. Shin, G.A. Bjarnason, D. Castellano, R.K. Silverman, R.F. Perini, C. Schloss, M.B. Atkins, Open-label, single-arm, phase II study of Pembrolizumab monotherapy as first-line therapy in patients with advanced non-clear cell renal cell carcinoma, J. Clin. Oncol. 39 (9) (2021) 1029–1039, https://doi.org/10.1200/jco.20.02365.

[34] M.A. Postow, J. Chesney, A.C. Pavlick, C. Robert, K. Grossmann, D. McDermott, G.P. Linette, N. Meyer, J.K. Giguere, S.S. Agarwala, M. Shaheen, M.S. Ernstoff, D. Minor, A.K. Salama, M. Taylor, P.A. Ott, L.M. Rollin, C. Horak, P. Gagnier, J.D. Wolchok, F.S. Hodi, Nivolumab and ipilimumab versus ipilimumab in untreated melanoma, N. Engl. J. Med. 372 (21) (2015) 2006–2017, https://doi.org/10.1056/NEJMoa1414428.

[35] L. Gandhi, D. Rodríguez-Abreu, S. Gadgeel, E. Esteban, E. Felip, F. De Angelis, M. Domine, P. Clingan, M.J. Hochmair, S.F. Powell, S.Y. Cheng, H.G. Bischoff, N. Peled, F. Grossi, R.R. Jennens, M. Reck, R. Hui, E.B. Garon, M. Boyer, B. Rubio-Viqueira, S. Novello, T. Kurata, J.E. Gray, J. Vida, Z. Wei, J. Yang, H. Raftopoulos, M.C. Pietanza, M.C. Garassino, Pembrolizumab plus chemotherapy in metastatic non-small-cell lung cancer, N. Engl. J. Med. 378 (22) (2018) 2078–2092, https://doi.org/10.1056/NEJMoa1801005.

[36] R.J. Motzer, N.M. Tannir, D.F. McDermott, O. Arén Frontera, B. Melichar, T.K. Choueiri, E.R. Plimack, P. Barthélémy, C. Porta, S. George, T. Powles, F. Donskov, V. Neiman, C.K. Kollmannsberger, P. Salman, H. Gurney, R. Hawkins, A. Ravaud, M.O. Grimm, S. Bracarda, C.H. Barrios, Y. Tomita, D. Castellano, B.I. Rini, A. C. Chen, S. Mekan, M.B. McHenry, M. Wind-Rotolo, J. Doan, P. Sharma, H.J. Hammers, B. Escudier, Nivolumab plus ipilimumab versus sunitinib in advanced renal-cell carcinoma, N. Engl. J. Med. 378 (14) (2018) 1277–1290, https://doi.org/10.1056/NEJMoa1712126.

[37] V.A. Boussiotis, Molecular and biochemical aspects of the PD-1 checkpoint pathway, N. Engl. J. Med. 375 (18) (2016) 1767–1778, https://doi.org/10.1056/NEJMra1514296.

[38] S.R. Gordon, R.L. Maute, B.W. Dulken, G. Hutter, B.M. George, M.N. McCracken, R. Gupta, J.M. Tsai, R. Sinha, D. Corey, A.M. Ring, A.J. Connolly, I. L. Weissman, PD-1 expression by tumour-associated macrophages inhibits phagocytosis and tumour immunity, Nature 545 (7655) (2017) 495–499, https://doi.org/10.1038/nature22396.

[39] Y. Wang, H. Ni, S. Zhou, K. He, Y. Gao, W. Wu, M. Wu, Z. Wu, X. Qiu, Y. Zhou, B. Chen, D. Pan, C. Huang, M. Li, Y. Bian, M. Yang, L. Miao, J. Liu, Tumor-selective blockade of CD47 signaling with a CD47/PD-L1 bispecific antibody for enhanced anti-tumor activity and limited toxicity, Cancer Immunol, Immunotherapy 70 (2) (2021) 365–376, https://doi.org/10.1007/s00262-020-02679-5.

[40] C.E. Demeure, H. Tanaka, V. Mateo, M. Rubio, G. Delespesse, M. Sarfati, CD47 engagement inhibits cytokine production and maturation of human dendritic cells, J. Immunol. 164 (4) (2000) 2193–2199, https://doi.org/10.4049/jimmunol.164.4.2193.

[41] L.W. Treffers, T. Ten Broeke, T. Rösner, J.H.M. Jansen, M. van Houdt, S. Kahle, K. Schornagel, P. Verkuijlen, J.M. Prins, K. Franke, T.W. Kuijpers, T.K. van den Berg, T. Valerius, J.H.W. Leusen, H.L. Matlung, IgA-mediated killing of tumor cells by neutrophils is enhanced by CD47-SIRPα checkpoint inhibition, Cancer Immunol. Res. 8 (1) (2020) 120–130, https://doi.org/10.1158/2326-6066.Cir-19-0144.

[42] L. Piccio, W. Vermi, K.S. Boles, A. Fuchs, C.A. Strader, F. Facchetti, M. Cella, M. Colonna, Adhesion of human T cells to antigen-presenting cells through SIRPbeta2-CD47 interaction costimulates T-cell proliferation, Blood 105 (6) (2005) 2421–2427, https://doi.org/10.1182/blood-2004-07-2823.

[43] H. Yang, R. Shao, H. Huang, X. Wang, Z. Rong, Y. Lin, Engineering macrophages to phagocytose cancer cells by blocking the CD47/SIRPα axis, Cancer Med. 8 (9) (2019) 4245–4253, https://doi.org/10.1002/cam4.2332.

[44] H.W. Mittrücker, A. Visekruna, M. Huber, Heterogeneity in the differentiation and function of CD8⁺ T cells, Arch. Immunol. Ther. Exp. 62 (6) (2014) 449–458, https://doi.org/10.1007/s00005-014-0293-y.

[45] S.M.G. Hayat, V. Bianconi, M. Pirro, M.R. Jaafari, M. Hatamipour, A. Sahebkar, CD47: role in the immune system and application to cancer therapy, Cell. Oncol. 43 (1) (2020) 19–30, https://doi.org/10.1007/s13402-019-00469-5.
[46] R. Advani, I. Flinn, L. Popplewell, A. Forero, N.L. Bartlett, N. Ghosh, J. Kline, M. Roschewski, A. LaCasce, G.P. Collins, T. Tran, J. Lynn, J.Y. Chen, J.P. Volkmer, B. Agoram, J. Huang, R. Majeti, I.L. Weissman, C.H. Takimoto, M.P. Chao, S.M. Smith, CD47 blockade by Hu5F9-G4 and rituximab in non-Hodgkin's lymphoma, N. Engl. J. Med. 379 (18) (2018) 1711–1721, https://doi.org/10.1056/NEJMoa1807315.
[47] M.P. Chao, A.A. Alizadeh, C. Tang, J.H. Myklebust, B. Varghese, S. Gill, M. Jan, A.C. Cha, C.K. Chan, B.T. Tan, C.Y. Park, F. Zhao, H.E. Kohrt, R. Malumbres, J. Briones, R.D. Gascoyne, I.S. Lossos, R. Levy, I.L. Weissman, R. Majeti, Anti-CD47 antibody synergizes with rituximab to promote phagocytosis and eradicate non-Hodgkin lymphoma, Cell 142 (5) (2010) 699–713, https://doi.org/10.1016/j.cell.2010.07.044.
[48] G.H.Y. Lin, V. Chai, V. Lee, K. Dodge, T. Truong, M. Wong, L.D. Johnson, E. Linderoth, X. Pang, J. Winston, P.S. Petrova, R.A. Uger, N.N. Viller, TTI-621 (SIRPαFc), a CD47-blocking cancer immunotherapeutic, triggers phagocytosis of lymphoma cells by multiple polarized macrophage subsets, PLoS One 12 (10) (2017) e0187262, https://doi.org/10.1371/journal.pone.0187262.
[49] E.C. Piccione, S. Juarez, S. Tseng, J. Liu, M. Stafford, C. Narayanan, L. Wang, K. Weiskopf, R. Majeti, Sirpα-antibody fusion proteins selectively bind and eliminate dual antigen-expressing tumor cells, Clin. Cancer Res. 22 (20) (2016) 5109–5119, https://doi.org/10.1158/1078-0432.Ccr-15-2503.
[50] R. Advani, J.P. Volkmer, M.P. Chao, CD47 blockade and rituximab in non-Hodgkin's lymphoma, N. Engl. J. Med. 380 (5) (2019) 497–498, https://doi.org/10.1056/NEJMc1816156.
[51] X. Liu, L. Liu, Z. Ren, K. Yang, H. Xu, Y. Luan, K. Fu, J. Guo, H. Peng, M. Zhu, Y.X. Fu, Dual targeting of innate and adaptive checkpoints on tumor cells Limits immune evasion, Cell Rep. 24 (8) (2018) 2101–2111, https://doi.org/10.1016/j.celrep.2018.07.062.
[52] X. Liu, Y. Pu, K. Cron, L. Deng, J. Kline, W.A. Frazier, H. Xu, H. Peng, Y.X. Fu, M.M. Xu, CD47 blockade triggers T cell-mediated destruction of immunogenic tumors, Nat. Med. 21 (10) (2015) 1209–1215, https://doi.org/10.1038/nm.3931.
[53] B. Liu, H. Guo, J. Xu, T. Qin, Q. Guo, N. Gu, D. Zhang, W. Qian, J. Dai, S. Hou, H. Wang, Y. Guo, Elimination of tumor by CD47/PD-L1 dual-targeting fusion protein that engages innate and adaptive immune responses, mAbs 10 (2) (2018) 315–324, https://doi.org/10.1080/19420862.2017.1409319.
[54] H. Ke, F. Zhang, J. Wang, L. Xiong, X. An, X. Tu, C. Chen, Y. Wang, B. Mao, S. Guo, C. Ju, X. He, R. Sun, L. Zhang, O.A. O'Connor, Q.X. Li, HX009, a novel BsAb dual targeting PD1 x CD47, demonstrates potent anti-lymphoma activity in preclinical models, Sci. Rep. 13 (1) (2023) 5419, https://doi.org/10.1038/s41598-023-32547-y.